Int. J. Electrochem. Sci., 16 **(2021)** Article ID: 210458, doi: 10.20964/2021.04.18

International Journal of
ELECTROCHEMICAL
SCIENCE
www.electrochemsci.org

Electrochemical Evaluation of MoS_2-Cu-RGO as a Catalyst for Hydrogen Evolution in Microbial Electrolysis Cell

Hongyan Dai[1,*], *Huimin Yang*[2], *Zhenhai Liang*[2]

[1] Department of Materials and Chemical Engineering, Taiyuan College, Taiyuan 030032, China
[2] College of Chemistry and Chemical Engineering, Taiyuan University of Technology, Taiyuan 030024, China
[*]E-mail: daihongyan12@sina.com

Received: 5 December 2020 / *Accepted:* 19 January 2021 / *Published:* 28 February 2021

A series of MoS_2-Cu-RGO composites were synthesized by hydrothermal method, and loaded on the carbon-based electrode. The best MoS_2-Cu-RGO electrode selected through electrochemical tests was applied as the cathode to produce hydrogen in a single-chamber microbial electrolysis cell (MEC). SEM and TEM images showed that most thin MoS_2 sheets vertically grew on the surface of RGO; Cu_2O acted as the bridged absorbent and efficient charge transfer channels between RGO and MoS_2, which exposed more hydrogen evolution active sites and improved the electrical conductivity. Electrochemical tests showed that the optimal mass ratio of $(NH_4)_2MoS_4$, GO and $CuCl_2 \cdot 2H_2O$ was 1:1:1.1, and 3 mg/cm^2 was the optimal load for carbon paper. The average current density, coulombic efficiency, hydrogen recovery efficiency, cathodic hydrogen recovery efficiency, hydrogen production rate, electrical recovery efficiencies and overall energy recovery efficiencies obtained with MoS_2-Cu-RGO cathode MEC were 10.28±0.40 A/m^2, 92.10±3.53%, 74.69±4.45%, 79.22±3.53%, 0.449±0.027 m^{3}H$_2$/m^{3}d, 237.68±15.66% and 88.20±5.60%, higher than those obtained with the Pt/C cathode MEC. The MoS_2-Cu-RGO cathode enjoyed good stability and price advantage, which might promote the practical application of MECs.

Keywords: MoS_2-Cu-RGO, carbon-based electrode, microbial electrolysis cell, hydrogen production.

1. INTRODUCTION

H_2 is an ideal clean energy source and widely used in many industrial chemical processes[1,2]. Traditional hydrogen production technology consumes a large amount of fossil fuels and suffers from serious carbon dioxide emission, which is not recommended. As a relatively novel bioelectrochemical technology, microbial electrolysis cell (MEC) can produce hydrogen gas with a small voltage input and meanwhile decompose organic compounds through microbial activity[3]. Due to the relatively low

consumption of energy for hydrogen production and sustainable treatment of wastewater, the MEC technology has a promising prospects in the industry[4].

The cathode of MEC has a great influence on hydrogen production. A perfect cathode has low hydrogen over-potential, good electrocatalytic activity, electrochemical stability and high corrosion resistance[5]. Pt group metals are regarded as the ideal catalyst for hydrogen evolution reactions (HER), but expensive, scarce[6]and, in addition, easily poisoned by some chemicals in wastewater (such as sulfides)[7].

Since Hinnemann et al discovered that the binding energy of MoS_2 to hydrogen atoms closed to that of Pt[8], the hydrogen evolution performance of MoS_2 was widly researched[9-12]. The number of active edge sites has a significant influence on the HER activity of MoS_2 [13,14]. However, the vertical S-Mo-S interlayers structure of bulk MoS_2 sharply reduces the amount of the exposed active sites and results in the poor conductivity[15,16]. In order to maximize the amount of catalytic active sites, bulk MoS_2 can be downsized to nanoparticles or even the discrete clusters[17,18]. Further more, loading MoS_2 nanoparticles onto graphene or other carbon materials can significantly increase the amount of exposed edge active sites, improve the electrical conductivity, and thereby improve the catalytic capacity of HER[19,20]. In our previous studies, MoS_2 was loaded on reduced graphene oxide (RGO) by hydrothermal method and utilized as the HER catalyst in MEC. The functional groups of RGO can facilitate the bonding process of RGO and MoS_2 to form a stable chemical linkage for electron transfer to accelerate the electron transfer[21]. The results showed that the catalytic effect of this compound was better than that of Pt[22]. However, it had been pointed out that the negatively charged oxygen-containing functional groups of graphene oxide (GO) repel the precursor of Mo (MoO_4^{2-} or $Mo_7O_{24}^{6-}$), leading to the random distributed agglomeration of MoS_2[21], which might affect the connectivity between RGO and MoS_2 [23].Therefore, some modifications were used to improve the interphase connectivity between RGO and MoS_2[24,25]. In some water electrolysis studies, the metal cations were introduced into MoS_2 though chemical doping to form M-Mo-S structures. The heteroatom-doped MoS_2 structures can adjust the electron density of MoS_2, reduce the bandgap, improve the conductivity, and offer more active sites for HER[26]. Especially the electron synergy between atoms can also weaken S-Hads bonds, which can optimize the adsorption and desorption of H [27]. However, there are barely any study on metal ions as improver of the heteroatom-doped MoS_2/RGO in the academic field of MEC.

In this paper, a series of MoS_2-Cu-RGO composites with different amounts of Cu was synthesized through a facile in-situ hydrothermal method. The optimum ratio of the raw materials and the optimum load on the carbon paper were estimated through electrochemical tests. Finally, the best electrode was applied to produce hydrogen in MEC, and compared with Pt/C electrode (Pt 0.5 mg/cm^2) cathode in terms of current densities and hydrogen production rate.

2. MATERIAL AND METHODS

2.1 MoS_2-Cu-RGO composites synthesis

A series of MoS_2-Cu-RGO composites (1#-7#) were synthesized as follows: Firstly, 40mg GO powder, which was synthesized by modified Hummers method[28], was dispersed in 40mL distilled

water through ultrasonic vibration for 1 h to obtain the homogeneous solution. Secondly, a certain amount of $CuCl_2 \cdot 2H_2O$ (1# 0mg, 2# 11mg, 3# 22mg, 4# 33mg, 5# 44mg, 6# 55mg, 7# 66mg) was dissolved in the solution and stirred for 0.5h. Thirdly, $(NH_4)_2MoS_4$ (40mg) was added into the solution and treated with ultrasound for 0.5 hour. Then, hydrazine hydrate (HHA, 2 mL) was added to the solution and stirred for a few minutes. Finally, the solution was transferred to a stainless-steel high pressure reactor (100mL) and held at 180°C for 12 hours. The black product obtained from the high pressure reactor was centrifuged and washed with deionized water and anhydrous ethanol. After removing all the impurities, the black product was dried in a vacuum drying oven for 12 h (60 ºC).

2.2 Cathode electrode preparation

The cathodes were prepared according to the previous literature[3,22]. The electrode with a load of 1mg/cm^2 composite was firstly prepared and tested through linear sweep voltammetry (LSV). After picking out the best MoS_2-Cu-RGO composite, the optimal performance conditions were determined by varying the loading amount (0.5, 1, 2, 3, 4, 5 mg/cm^2). Then, the optimum MoS_2-Cu-RGO electrode was used as the cathode of MEC to test its hydrogen production performance

2.3 MEC construction and operation

The MEC used in this study was a single-chamber reactor with a working volume of 80 mL. The carbon felt biological anode(2×4×1 cm^3) was from the previous MECs, which had been running for more than one year. The cathode was the MoS_2-Cu-RGO carbon paper electrode(2×2 cm^2) prepared in 2.2. The anode was 1.5 cm from the cathode. 20 mL bacteria solution from previous MECs and 50 mL nutrient solution were then injected into the MEC. The composition of nutrient solution was same as previously described[22].

The MEC operated in fed-batch mode with an additional voltage of 0.7V. 50mL nutrient solution was replaced when the current of MEC dropped below 0.5mA and then sparged with N_2 for 15 min[29]. Meanwhile, the electrodes were exposed to air for 20–30 min to prevent methanogens from growing. All batch experiments were operated at room temperature (20 ºC) and run in duplicate.

2.4 Measurement and analysis

The morphologies and chemical composition of the composite samples were investigated by scanning electron microscope(SEM, JSM-7001F, JEOL, Japan), transmission electron microscopy (TEM, G2 F20, FEI, USA), and aperture analysis tester (ASAP-2000, USA). The element valence analysis was characterized by X-ray photoelectron spectroscopy (XPS, K-alpha, Thermo, UK) using a Mg-Kα X-ray source. LSV and Tafel analysis of the MoS_2-Cu-RGO electrode were carried out on an electrochemical workstation (Princeton Applied Research, USA). A three-electrode system was used in the test, with MoS_2-Cu-RGO electrode as working electrode, Pt electrode as counter electrode and saturated calomel electrode (SCE) as reference electrode. The electrolyte was phosphoric acid buffer

solution of 100 mM with the pH of 7. LSV curves and Tafel plots were measured with a sweep rate of 10 mV/s. In the manuscript, all the potentials were against the reversible hydrogen electrode (RHE): E(RHE)=E(SCE)+0.241+0.0591pH.

A digital multimeter (UNI-T 803; Uni-Trend Electronics Co., Ltd., Shanghai, China) was used to record the current of the MEC every 30 min. The gas production and composition of MEC were determined using the methods described by Dai[3]. The coulombic efficiency (R_{CE}), hydrogen recovery efficiency (R_{H2}), cathodic hydrogen recovery efficiency (R_{cat}), hydrogen production rate (Q_{H2}), and energy recovery efficiencies (electrical and overall energy, η_W and η_{W+S}) of MEC were calculated as previously described[30].

3. RESULTS AND DISCUSSIONS

3.1 Chemical morphology and composition characterization

The micro-morphologies of the prepared composites were characterized by SEM and TEM images (Fig. 1). From the SEM image of pure MoS_2 (Fig. 1A), it can be seen that MoS_2 had a block-like structure. The prepared MoS_2-Cu-RGO composite had obvious three-dimensional layered structure (Fig. 1B). Most thin MoS_2 sheets vertically grew on the surface of RGO, greatly building up the certain surface area of the material, which facilitated more hydrogen evolution active site exposure. It is shown in Fig. 1C that MoS_2 was dispersed on the graphene surface. As labeled in Fig. 1D, clear lattice spacings of around 0.625nm, 0.25nm and 0.34nm were obtained, which corresponded to the crystallographic (002) spacing of MoS_2[6], (111) spacing of Cu_2O[31] and (002) spacing of RGO[6]. Clear lattice fringes showed that the prepared composite had a crystal structure. More importantly, Cu_2O acted as the bridged absorbent and efficient charge transfer channels between RGO and MoS_2, which could prevent MoS_2 from clustering on RGO, and uniformly dispersed it on RGO surface, thereby increasing exposed hydrogen evolution active sites and improving conductivity.

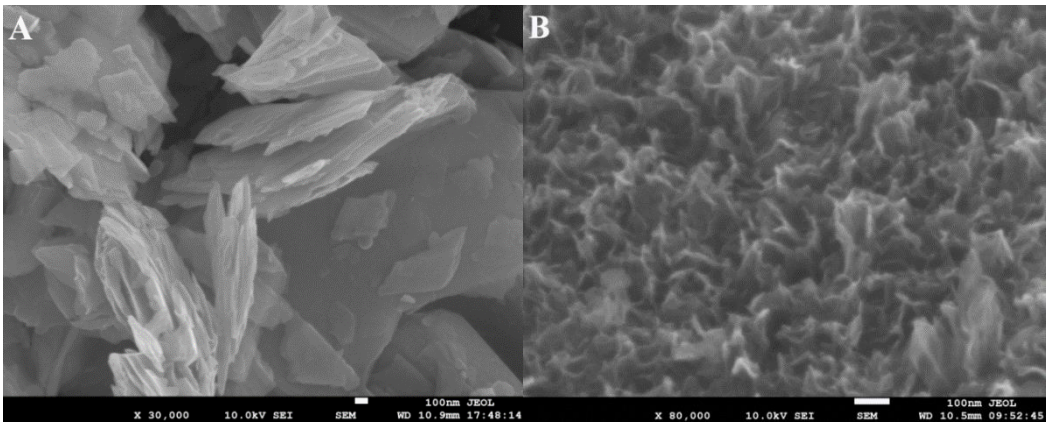

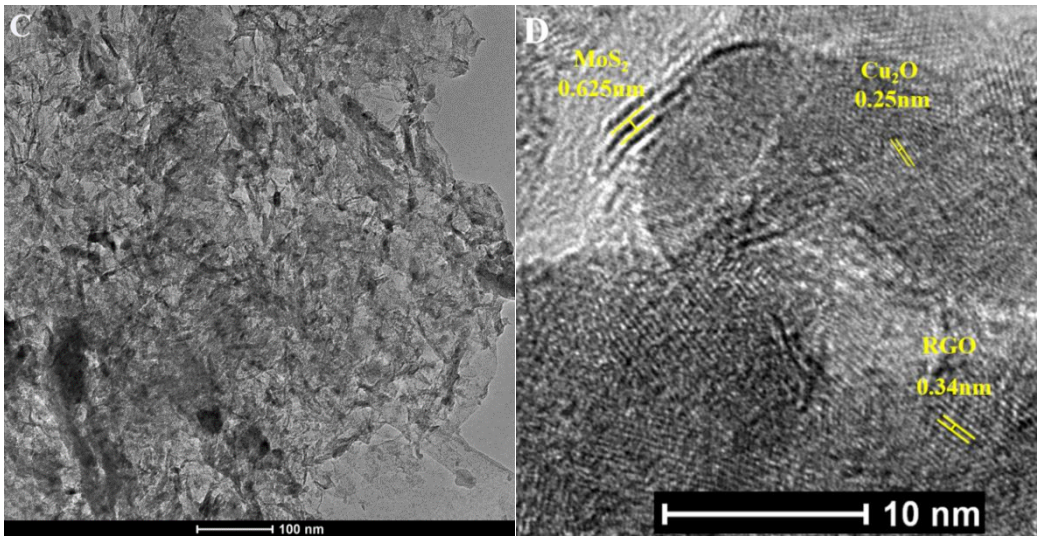

Figure 1. The SEM images of MoS_2 (A), 5# MoS_2-Cu-RGO(B), and the TEM images of 5# MoS_2-Cu-RGO(C, D).

XRD pattern revealed the crystal structure of MoS_2-Cu-RGO (Fig. 2). As we all know, the characteristic peak of GO appears around 10°. However, in Fig.2, the characteristic peak was absent. Instead, a diffraction peak representing RGO appeared at 18.8°, which might be ascribed to the formation of ‘‘re-graphitized’’ carbon regions and restacking due to the attractive interactions between RGO and metal ions[32]. The diffraction peak at 29.4° could be assigned to the (110) planes of Cu_2O (JCPDS No. 99-0041). Two diffraction peaks at 33° and 48° could be assigned to the (100) and (105) planes of MoS_2 (JCPDS No. 37-1492). The disappearance of the diffraction peaks at high 2θ region revealed the disordered structure of MoS_2.

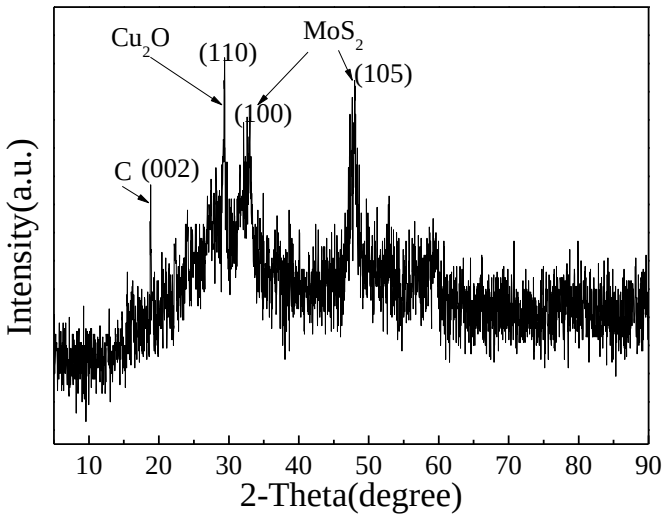

Figure 2. XRD pattern of 5# MoS_2-Cu-RGO

The chemical states of different elements in the MoS_2-Cu-RGO were analyzed by XPS spectroscopy. As shown in the survey spectrum of Fig. S1, the elements of C, O, S, Mo and Cu could be clearly identified, and there were no other impurities. The result was consistent with that of the energy dispersive spectrometer (EDS). In the XPS spectrum of MoS_2-Cu-RGO of C 1s (Fig. 3A), there were two characteristic peaks, with one at 284.77 eV assigned to C-C bonding and the other at 285.9 eV assigned to C-O/C-O-C bonding [33, 34]. In the high-resolution spectrum of Mo 3d (Fig. 3B), five fitted peaks were obtained. Two peaks observed at around 233 and 229 eV were corresponding to the Mo $3d_{3/2}$ and Mo $3d_{5/2}$ of Mo^{4+} in MoS_2[35].

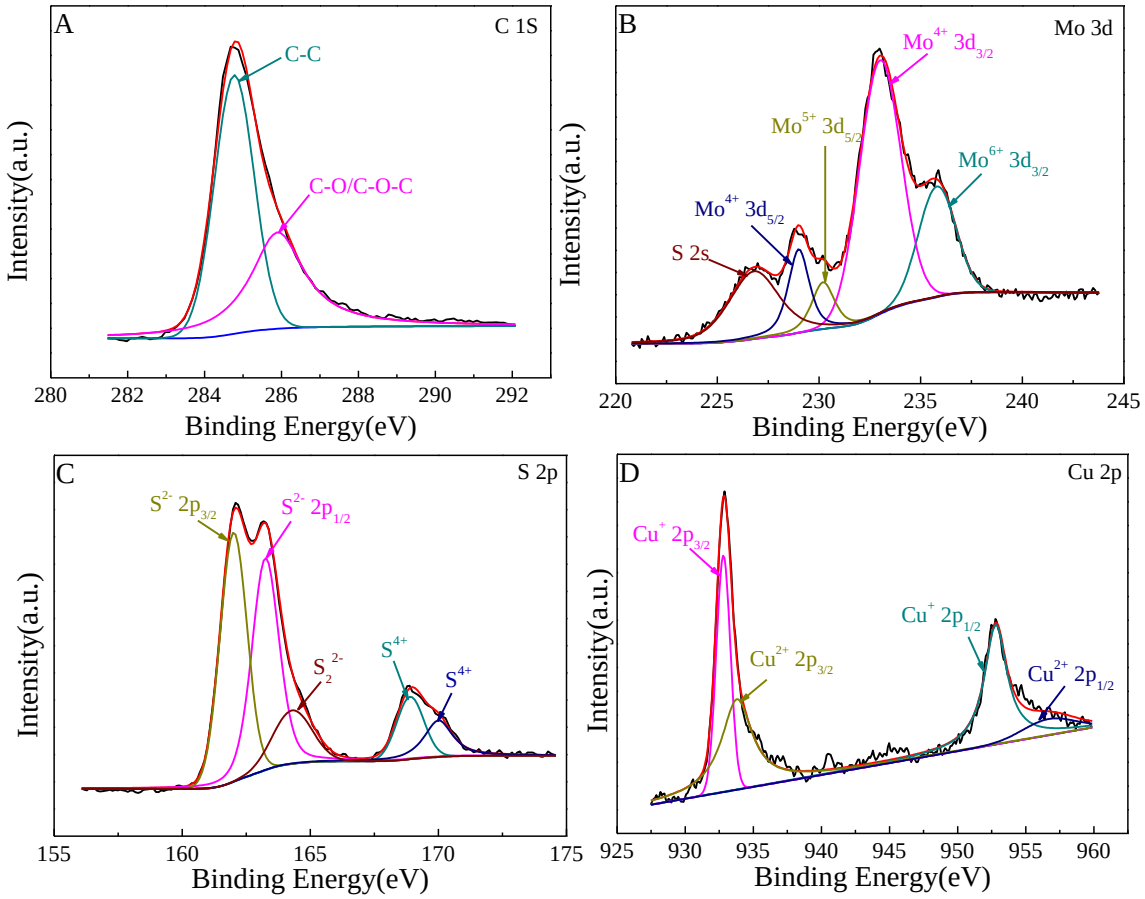

Figure 3. The high resolution XPS spectra of (A) C 1s spectrum, (B) Mo 3d spectrum, (C) S 2p spectrum, (D) Cu 2p spectrum for MoS_2-Cu-RGO.

The peak at about 235.8 eV could be assigned to Mo^{6+} $3d_{3/2}$ due to the presence of MoO_3 or MoO_4^{2+}, which might result from the oxidation of the compound by oxygen and unreacted materials[36]. The peak at about 230.2 eV could be assigned to Mo^{5+} $3d_{5/2}$, which might be reduced from Mo^{6+} in the sulfide intermediate phases[35]. The peak at about 226.8 eV was attributed to S 2s of MoS_2[35]. In S 2p of Fig. 3C, the two peaks at around 162 and 163.3 eV could be ascribed to the S $2p_{3/2}$ and S $2p_{1/2}$ of S^{2-}, respectively[37]. The peak located at binding energy of 164.3 eV indicated the existence of S_2^{2-} and/or S^{2-}[38], which might have a good catalytic effect on the hydrogen evolution reaction. The last two peaks

centered at about 168.9 and 170 eV might be the S^{4+} species in SO_3^{2-}, which presented at edges of MoS_2 layers[39]. There were four peaks in the high-resolution spectrum of Cu 2p (Fig. 3D). The two main peaks centered at 932.8 and 952.8 eV could be assigned as Cu $2p_{3/2}$ and Cu $2p_{1/2}$ of Cu^+ in Cu_2O, respectively[40]. The other two peaks located at 933.8 and 956.7 eV were attributed to Cu $2p_{3/2}$[31] and Cu $2p_{1/2}$[41] of Cu^{2+} in CuO, respectively, which confirmed the existence of CuO in the compound.

3.2 Electrochemical properties of the composites

To evaluate the electrocatalytic properties of the as-prepared catalysts for HER, the LSV and tafel analysis were performed on different samples (1#-7#). Before testing, the different prepared catalysts were loaded on carbon paper with a loading of 1mg/cm^2. We can see from Fig.4A, within the scanning range of below -0.5V(vs.RHE), as the amount of Cu added to the catalyst increasing, the hydrogen evolution catalytic capacity of MoS_2-Cu-RGO electrodes firstly increased and then decreased and the current response of 5 # electrode was larger than other electrodes. For example, at the potential of -0.545 V (vs. RHE), the current density of 5# electrode was -105.4 A/m^2, much higher than those of the 1#(-79.50 A/m^2), 2# (-87.17A/m^2), 3# (-91.29A/m^2), 4# (-92.98 A/m^2), 6# (-96.45 A/m^2) and 7# (-90.39 A/m^2) electrode. The reasons for this phenomenon might be as follows: Because of the addition of Cu, MoS_2 was prevented from clumping and gathering on RGO. MoS_2 was more effectively dispersed on the surface of RGO to expose more catalytic active sites. In addition, Cu could adjust the electronic density and reduce the bandgap of MoS_2[42]. The synergistic effect of electrons between Cu, Mo, S could also weaken S−H ads bonds, which would optimize the adsorption and desorption of H [2]. When the ratio of Cu in the composite gradually increased, the effect of Cu gradually appeared. So the catalytic activity of the composite electrodes increased with the increase of cu content. However, when the proportion of Cu in the composite increased to a certain extent (e.g. 7#), there was too little MoS_2 in the compound, leading to a reduction of active sites and thus a drop in catalytic activity. In the range of -0.545 V (vs. RHE) to 0V (vs. RHE), the current density of the 5 # electrode was not much different from other MoS_2-Cu-RGO electrodes. Results indicated that the 5# MoS_2-Cu-RGO showed the best catalytic activity for HER.

After selecting the best catalyst through Figure 4A, the 5# composite was used at loads of 0.5, 1, 2, 3, 4 or 5 mg/cm^2 and investigated by LSV. For comparison, the Pt/C carbon paper electrode (0.5 mg/cm^2) was also evaluated. As shown in Fig. 4B, within the scanning range, as the load increased, the catalytic capacity of the MoS_2-Cu-RGO electrodes increased first and then decreased. The catalytic performance of the electrode with a load of 3mg/cm^2 was better than that of other electrodes. Moreover, the initial potential of hydrogen evolution of this electrode was less than that of other electrodes. Compared with Pt/C, the current responses of 5# MoS_2-Cu-RGO with the load of 3 mg/cm^2 were higher than that of Pt/C within the scanning range of -0.3 V-0.1 V (vs. RHE), and the initial potential of hydrogen evolution of it was also less than that of Pt/C.

The results showed that the 5# composite electrode at a load of 3 mg/cm^2 was the optimal MoS_2-Cu-RGO electrode.

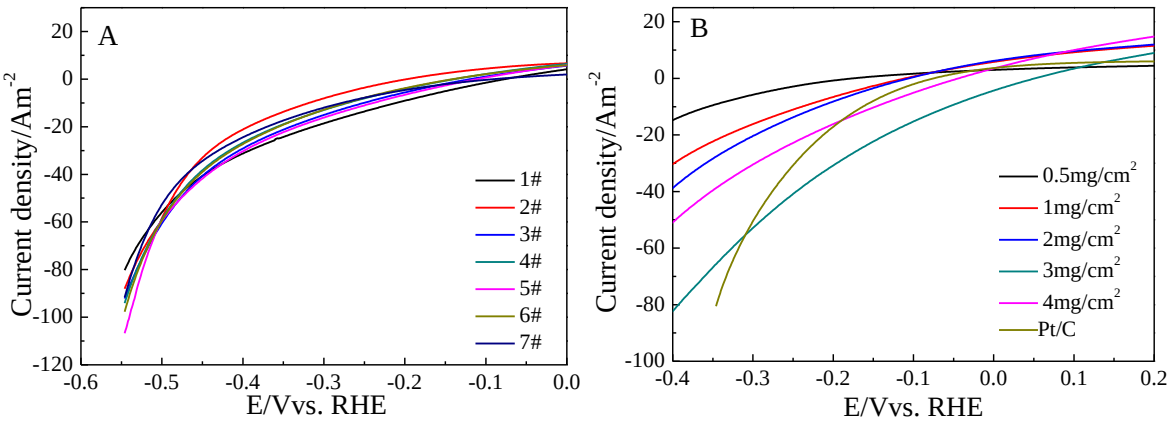

Figure 4. The LSV of 1#-7# composite electrodes with the load of 1mg·cm^{-2} (A) and the 6# composite electrodes with different loads (B).

Tafel slope is an inherent property of electrocatalysts. The smaller the Tafel slope of the catalyst, the faster HER rate[43]. The kinetics of hydrogen evolution under neutral conditions is slower than that under acidic conditions[44]. Tafel slope of Pt is 30 mV / dec under acidic conditions[45,46]. In this study, The Tafel slope of Pt/C electrode was 44.4mV/dec, which was greater than 30mV/dec. This result once again validated the conclusion that the rate of hydrogen evolution under neutral condition was slower than that under acidic condition. The tafel slope of MoS_2-Cu-RGO electrode (5#, 3mg/cm^2) was 41.2mV/dec, lower than that of MoS_2-RGO (1#) (54.9mV/dec), showing that the introduction of Cu into the compound was beneficial to improve the HER kinetics. The Tafel slope of MoS_2-Cu-RGO electrode was slightly lower than that of Pt/C, indicating that the HER rate of MoS_2-Cu-RGO was slightly faster than that of Pt/C.

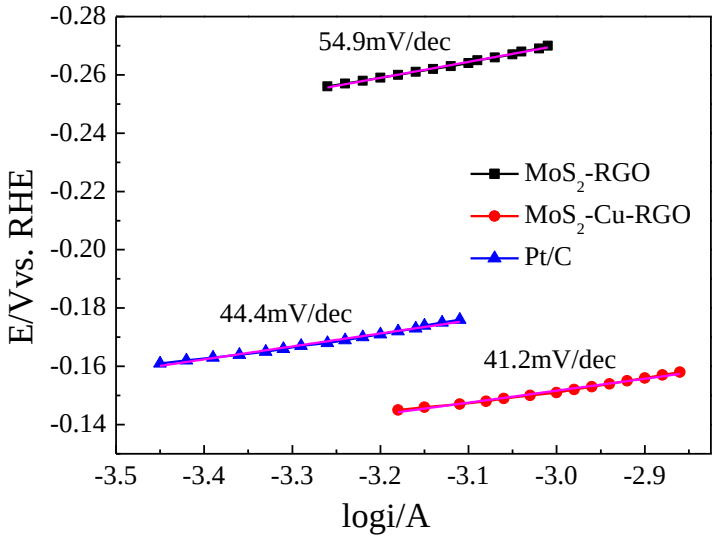

Figure 5. Tafel plots for MoS_2-RGO (1#), MoS_2-Cu-RGO (5#, 3mg/cm^2) and Pt/C electrodes.

Through electrochemical tests, it could be concluded that 5# MoS_2-Cu-RGO had the best catalytic activity for hydrogen evolution and the best catalyst load is 3 mg/cm^2. Therefore, in the subsequent MEC hydrogen production experiment, the carbon paper electrode modified with 5# MoS_2-Cu-RGO (3 mg/cm^2) was selected as the cathode of MEC.

3.3 MEC tests

The single-chamber MECs with MoS_2-Cu-RGO (5#, 3 mg/cm^2) cathode were operated with an added voltage of 0.7 V. For comparison, the MECs with Pt/C cathode were also running at the same time. Fig. 6 recorded the current densities of the MECs for 5 cycles. Similar to the results of others[47, 48], typical periodic current density changes were shown in Fig. 6. The average current density of MoS_2-Cu-RGO cathode MEC was 10.28±0.40 A/m^2, which was higher than that of Pt/C cathode MEC (9.29± 1.31 A/m^2). Furthermore, the peak current densities of MoS_2-Cu-RGO cathode MEC in 5 cycles were higher than that of the Pt/C cathode MEC, indicating that MoS_2-Cu-RGO had good hydrogen evolution catalytic activity. In addition, the periodic current densities of MoS_2-Cu-RGO cathode MEC were very stable, revealing the good stability of MoS_2-Cu-RGO. After 2 months of operation, the peak current densities of MoS_2-Cu-RGO cathode MEC was 16.35±0.85 A/m^2, demonstrating that the catalytic activity of the catalyst did not decrease after long-term operation, which was beneficial to practical application. The peak current densities of Pt/C cathode MEC decreased. The reason might be that Pt was poisoned by the phosphorus ions in the nutrient solution[49].

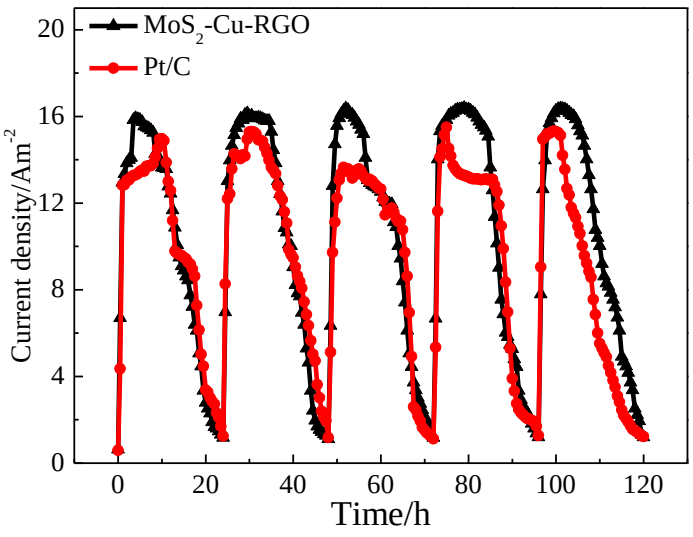

Figure 6. Current generation for MoS_2-Cu-RGO and Pt/C cathodes in the MECs (The applied voltage was 0.7V).

The gas produced by MEC each cycle was collected using drainage method. A gas chromatograph was utilized to analyze its composition. The R_{CE}, R_{H2}, R_{cat}, Q_{H2}, η_W and η_{W+S} of MECs

with MoS_2-Cu-RGO or Pt/C cathode were calculated. All results were tabulated in Table 1. The gas produced by the MoS_2-Cu-RGO cathode MEC was 55.80±2.60 mL/cycle, which was higher than that by Pt/C cathode MEC (48.85±4.55 mL/cycle) and MoS_2/graphene cathode MEC (52.65±4.15 mL/cycle)[22], indicating that the catalytic activity of MoS_2-Cu-RGO for hydrogen evolution was better than that of Pt/C or MoS_2/graphene. The proportion of H_2 produced by the MoS_2-Cu-RGO cathode MEC totaled 63.39±1.46%, which was slightly higher than that of Pt/C cathode MEC (60.29±4.01%). The CO_2 composition of the former (27.23±1.92%) was similar with that of the latter (28.36±4.76%). The CH_4 percentage produced by the latter (10.70±2.10%) was higher than that produced by the former (8.04±2.34%). The CH_4 in the gas was produced by hydrogenotrophic methanogenesis. In the latter part of the reaction cycle, nutrients were depleted, and the H_2 concentration was high, which led to the consumption of H_2 by hydrogenotrophic methanogenesis and the synthesize of CH_4 [50]. Shortening the batch cycle might reduce the content of CH_4. As shown in Table 1, the performance of MoS_2-Cu-RGO cathode MEC was superior to that of Pt/C cathode MEC in terms of R_{CE} (92.10±3.53% vs. 83.19±11.77%), R_{H2} (74.69±4.45% vs. 62.75±8.67%), R_{cat} (79.22±3.53% vs. 71.40±9.03%), Q_{H2} (0.449±0.027 m^3H_2/m^3d vs. 0.377±0.052 m^3H_2/m^3d), η_W (237.68±15.66% vs. 228.39±18.91%) and η_{W+S} (88.20±5.60% vs. 83.46±10.16%), demonstrating that MoS_2-Cu-RGO had excellent catalytic activity. The performance of MoS_2-Cu-RGO cathode MEC was also superior to that of MoS_2/graphene MEC[22], further clarifying the importance of Cu in the composite. Compared with other non-noble metal hydrogen evolution catalysts (such as stainless steel fiber felt[51], NiW/Ni-foam[52] et al) studied by other researchers, the performance of MoS_2-Cu-RGO was better than those, indicating its excellent catalytic properties.

Table 1. Summary of results from the MECs for MoS_2-Cu-RGO and Pt/C cathodes at applied voltage of 0.7V.

	Q_{gas} (mL /cycle)	H_2(%)	CH_4(%)	CO_2(%)	Q_{H2} (m^3H_2/m^3d)
Pt/C	48.85±4.55	60.29±4.01	10.70±2.10	28.36±4.76	0.377±0.052
MoS_2-Cu-RGO	55.80±2.60	63.39±1.46	8.04±2.34	27.23±1.92	0.449±0.027
	R_{CE}(%)	R_{H2}(%)	R_{cat}(%)	η_W(%)	η_{W+S}(%)
Pt/C	83.19±11.77	62.75±8.67	71.40±9.03	228.39±18.91	83.46±10.16
MoS_2-Cu-RGO	92.10±3.53	74.69±4.45	79.22±3.53	237.68±15.66	88.20±5.60

During the two months experiment, the performance of the MoS_2-Cu-RGO cathode remained stable. More importantly, the production cost of MoS_2-Cu-RGO cathode was lower than Pt/C cathode. It was estimated that the cost of the MoS_2-Cu-RGO cathode was twenty times less than that of the Pt/C cathode, thus, increasing the practical application of MECs.

4. CONCLUSION

A series of MoS_2-Cu-RGO composites were synthesized by hydrothermal method. SEM image showed that most thin MoS_2 sheets vertically grew on the surface of RGO, significantly increasing the specific surface area of the material. TEM images showed that Cu_2O acted as the bridged absorbent and efficient charge transfer channels between RGO and MoS_2, which increased exposed hydrogen evolution active sites and improved conductivity. Electrochemical test showed that when the mass ratio of $(NH_4)_2MoS_4$, GO and $CuCl_2 \cdot 2H_2O$ was 1:1:1.1, the synthetic composite demonstrated the best catalytic performance. 3 mg/cm^2 was the optimal load for carbon paper. In the MEC experiment, the MoS_2-Cu-RGO cathode MEC performed better than that of Pt/C cathode MEC in terms of average current density, hydrogen production rate, hydrogen recovery efficiency and energy recovery efficiencies. More importantly, the MoS_2-Cu-RGO cathode exhibited good stability and price advantage. Thus, MoS_2-Cu-RGO cathode could be considered as cost-effective and highly efficient alternatives for Pt catalyst in MECs.

SUPPLEMENTARY INFORMATION

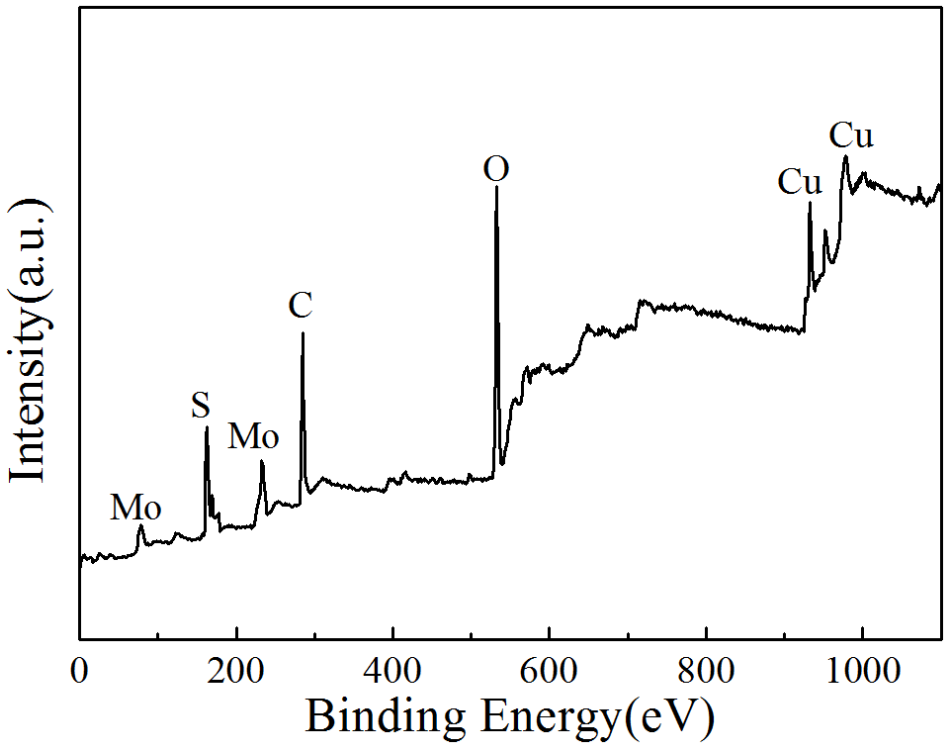

Figure S1. The XPS survey spectrum of MoS_2-Cu-RGO

ACKNOWLEDGEMENTS
This work is co-funded by the University Science and Technology Innovation Program of Shanxi Province (Grant No. 2019L1006) and the National Natural Science Foundation of China (Grant No. 51703151).

References

1. C.T. Dinh, A. Jain, F. Pelayo García de Arquer, P.D. Luna , J. Li, N. Wang, X. L. Zheng, J. Cai, B. Z. Gregory, O. Voznyy, B. Zhang, M. Liu, D. Sinton , E. J. Crumlin, and E. H. Sargent. *Nature Energy*, 4 (2019) 107.
2. J.X. Feng, J.Q. Wu, Y.X. Tong, and G.R. Li. *Journal of the American Chemical Society*, 140(2) (2018) 610.
3. H.Y. Dai, H.M. Yang, X. Liu, X. Jian, and Z.H. Liang. *Fuel,* 174 (2016) 251.
4. F.J. Li, W.F. Liu, Y. Sun, W.J. Ding, and S.A. Cheng. *International Journal of Hydrogen Energy*, 42 (2017) 3641.
5. C. Lupi, A. Dell'Era, and M. Pasquali. *International Journal of Hydrogen Energy*, 39 (2014) 1932.
6. B.H. He, L. Chen, M.J. Jing, M.J. Zhou, Z.H. Hou, and X.B. Chen. *Electrochim Acta*, 283 (2018) 357.
7. A. Kundu, J.N. Sahu, G. Redzwan, and M.A. Hashim. *International Journal of Hydrogen Energy*, 38 (2013) 1745.
8. B. Hinnemann, P.G. Moses, J. Bonde, K.P. Jørgensen, J.H. Nielsen, S. Horch, I. Chorkendorff, and J. K. Nørskov. *Journal of the American Chemical Society*, 127(15) (2005) 5308.
9. P. Zhu, Y. Chen, Y. Zhou, Z.X. Yang, D. Wu, X. Xiong, and F.P. Ouyang. *International Journal of Hydrogen Energy*, 43 (2018) 14087.
10. Z.C. Xiang, Z. Zhang, X.J. Xu, Q. Zhang, and C.W. Yuan. *Carbon*, 98 (2016) 84.
11. J. Deng, W.T. Yuan, P.J. Ren, Y. Wang, D.H. Deng, Z. Zhang, and X. H. Bao. *RSC Advances*, 4 (2014) 34733.
12. J.C. Tokash, and B.E. Logan. *International Journal of Hydrogen Energy*, 36 (2011) 9439.
13. G.Q. Li, D. Zhang, Q. Qiao, Y.F. Yu, D. Peterson, A. Zafar, R. Kumar, S. Curtarolo , F. Hunte, and S. Shannon. *Journal of the American Chemical Society*, 138(51) (2016) 16632.
14. S. Geng, W.W. Yang, and Y.S. Yu. *Journal of Catalysis*, 375 (2019) 441.
15. A.B. Laursen, S. Kegnaes, S. Dahl, and I. Chorkendorff. *Energy Environmental Science*, 5 (2012) 5577.
16. D.S. Kong, H.T. Wang, J.J. Cha, M. Pasta, K.J. Koski, J. Yao , and Y. Cui. *Nano Letters*, 13 (2013) 1341.
17. Y.G. Li, H.L. Wang, L.M. Xie, Y.Y. Liang, G.S. Hong, and H.J. Dai. *Journal of the American Chemical Society*, **133** (2011) 7296.
18. Z. Ji, C.A. Trickett, X.K. Pei, and O.M. Yaghi. *Journal of the American Chemical Society*, 140(42) (2018) 13618.
19. W.H. Hu, X. Shang, G.Q. Han, B. Dong, Y.R. Liu, X. Li, Y.R. Liu, X. Li, Y.M. Chai, Y.Q. Liu, and C.G. Liu. *Carbon*, 100 (2016) 236 .
20. Z.C. Xiang, Z. Zhang, X.J. Xu, Q. Zhang, and C.W. Yuan. *Carbon*, 98 (2016) 84 .
21. R.Y. Ge, W.X. Li, J.J. Huo, T. Liao, N.Y. Cheng, Y. Du, M.Y. Zhu, Y. Li, and J.J. Zhang. *Applied Catalysis B: Environmental*, 246 (2019) 129.
22. H.Y. Dai, H.M. Yang, X. Liu, X. Jian, M.M. Guo, L.L. Cao, and Z.H. Liang. *Chemical Journal of Chinese Universities*, 39(2) (2018) 351 .
23. Q. Quan, S.J. Xie, B. Weng, Y. Wang, and Y.J. Xu. *Small*, 14(21) (2018) 1870096.
24. L. Chen, G.S. Shi, J. Shen, B.Q. Peng, B.W. Zhang, Y.Z. Wang, F.G. Bian, J.J. Wang, D.Y. Li, Z. Qian, G. Xu, G.P. Liu, J.R. Zeng, L.J. Zhang, Y.Z. Yang, G.Q. Zhou, M.H. Wu, W.Q. Jin, J.Y. Li,

and H.P. Fang. *Nature* 550 (2017) 380.
25. M.B. Askari, A. Beheshti-Marnani, M. Seifi, S.M. Rozati, and P. Salarizadeh. *Journal of Colloid and Interface Science*, 537 (2019) 186 .
26. Y. Shi, Y. Zhou, D.R. Yang, W.X. Xu, F.B. Wang, J.J. Xu, X.H. Xia, and H.Y. Chen, *Journal of the American Chemical Society*, 139 (2017) 15479 .
27. J.X. Feng, J.Q. Wu, Y.X. Tong, and G.R. Li. *Journal of the American Chemical Society*, 140 (2018) 610 .
28. S. Stankovich, D.A. Dikin , G.H.B. Dommett, K.M. Kohlhass, Z.J. Zimney, and E.A. Stach. *Nature,* 442 (2006) 282.
29. D. Call, and B.E. Logan. *Environmental Science and Technology*. 42 (2008) 3401.
30. B.E. Logan, D. Call, S. Cheng, H.V.M. Hamelers, T.H.J.A. Sleutels, and A.W. Jere miasse. *Environmental Science and Technology,* 42 (2008) 8630.
31. X. Liu, X. Jian, H.M. Yang, X.L. Song, and Z.H. Liang. *New Journal of Chemistry*, 40(2016) 3075.
32. R.F. Nie, J.H. Wang, L.N. Wang, Y. Qin, P. Chen, and Z.Y. Hou. *Carbon*, 50 (2012) 586.
33. Y.Z. Lu, Y.Y. Jiang, W.T. Wei, H.B. Wu , M.M. Liu, L. Niu, and W. Chen. *Journal of Materials Chemistry,* 22 (2012) 2929.
34. M.M. Liu, and W. Chen. *Nanoscale*, 5 (2013) 12558.
35. W.H. Hu, X. Shang, G.Q. Han, B. Dong, Y.R. Liu, X. Li, Y.M. Chai, Y.Q. Liu, and C.G. Liu. *Carbon*, 100 (2016) 236.
36. F. Li, Li J, X.Q. Lin, X.Z. Li, Y.Y. Fang, L.X. Jiao, X.C. An, Y. Fu, J. Jin, and R. Li. *Journal of Power Sources*, 300 (2015) 301.
37. Y. Yan, X.M. Ge, Z.L. Liu, J.Y. Wang, J.M. Lee, and X. Wang. *Nanoscale*, 5(17) (2013) 7768.
38. V. Heron, M. Daniel, and H. Xile. *Energy & Environmental Science*, 5 (2012) 6136.
39. X.L. Zheng, J.B. Xu, K.Y. Yan, H. Wang, Z.L. Wang, and S.H. Yang. *Chemistry of Materials*, 26 (2014) 2344.
40. Z.Z. Wu, H. Fei, and D.Z. Wang. *Materials Letters*, 256 (2019) 126622.
41. F. Li, L. Zhang, J. Li, X.Q. Lin, X.Z. Li, Y.Y. Fang, J.W. Huang, W.Z. Li, M. Tian, J. Jin, and R. Li. *Journal of Power Sources*, 292 (2015) 15.
42. Y. Shi, Y. Zhou, D.R. Yang, W.X. Xu, C. Wang, F.B. Wang, J.J. Xu, X.H. Xia, and H.Y. Chen. *Journal of the American Chemical Society*, 139 (2017) 15479.
43. M. Daniel, and H. Xile. *Energy & Environmental Science*, 4(10) (2011) 3878.
44. L. Lu, D.X. Hou, Y.F. Fang, Y.P. Huang, and Z.Y.J. Ren. *Electrochimica Acta*, 206 (2016) 381.
45. Y.G. Li, H.L. Wang, L.M. Xie, Y.Y. Liang, G.S. Hong, and H.J. Dai. *Journal of the American Chemical Society*, 133 (2011) 7296.
46. D.S. Kong, H.T. Wang, Z.Y. Lu, and Y. Cui. *Journal of the American Chemical Society*, 136 (2014) 4897.
47. J.C. Tokash, and B.E. Logan. *International journal of hydrogen energy*, 36 (2011) 9439.
48. M. Su, L.L. Wei, Z.Z. Qiu, G. Wang, and J.Q. Shen. *Journal of Power Sources*, 301 (2016) 29.
49. L. De Silva Muňoz, A. Bergel, D. Féron, and R. Basséguy. *International journal of hydrogen energy,* 35 (2010) 8561.
50. A.J. Wang, W.Z. Liu, S.A. Cheng, D.F. Xing, J.Z. Zhou, and B.E. Logan. *International journal of hydrogen energy*, 34 (2009) 3653.
51. M. Su, L.L. Wei, Z.Z. Qiu, G. Wang, and J.Q. Shen. *Journal of Power Sources*, 301 (2016) 29.
52. M. Mitov, E. Chorbadzhiyska, L. Nalbandian, and Y. Hubenova. *Journal of Power Sources*, 356 (2017) 467.